ORNL/TM--9369

DE86 007077

ORNL/TM-9369
Dist. Category UC-20

Fusion Energy Division

EFFECT OF MAGNETIC BENDING ON THE EBT HIGH-FREQUENCY MODES

A. M. El-Nadi*
S. Hiroe
J. C. Whitson
H. F. Hassen*
H. A. Kirolous*

Date Published - February 1986

*Cairo University, Giza, Egypt

Prepared by the
OAK RIDGE NATIONAL LABORATORY
Oak Ridge, Tennessee 37831
operated by
MARTIN MARIETTA ENERGY SYSTEMS, INC.
for the
U.S. DEPARTMENT OF ENERGY
under Contract No. DE-AC05-84OR21400

CONTENTS

ABSTRACT

The high-frequency stability of the ELMO Bumpy Torus (EBT) device is studied when the wave vector has a finite component along the magnetic field lines. Unstable modes exist for any finite hot electron density.

I. INTRODUCTION

The ELMO Bumpy Torus (EBT) device is characterized by the presence of hot electron rings at the location where the frequency of the applied microwave power matches the local second harmonic electron cyclotron resonance.[1] The average poloidal magnetic precession frequency of the hot electrons, $\langle\omega_p\rangle$, is of the same order as the ion cyclotron frequency Ω_{ci}. The negative energy wave associated with this precession can couple with any positive energy wave having the same frequency and wave vector, thus giving rise to various instabilities.[2] Three possible candidates having positive energy are the high-frequency surface wave, the compressional wave, and the shear Alfvèn wave.[2-4] The coupling process has been studied for the first two waves in the flute limit using a radial analysis, and it was shown that stability imposes maximum thresholds both on the ratio of the hot electron to core ion densities and on the ion density itself.[3,4] The related instabilities are usually denoted by the hot interchange and the compressional Alfvèn instability, respectively. The T-M transition, in which a significant drop in the stored energy of the rings occurs, is usually considered to be related to the hot interchange instability, since both the threshold and the orientation of the perturbed magnetic field along the equilibrium magnetic field are in good agreement with theory. Recently, the coupling of the ring precession to the shear Alfvèn waves has received more attention through both radial and axial analyses.[3,4]

Another type of high-frequency fluctuation, characterized by the presence of a poloidal magnetic component in addition to the compressional component, has been recently detected. It is usually present at hot electron densities too small to trigger the interchange mode, and the unstable frequency spectrum is much higher than the ion cyclotron frequency. If we ignore the parallel component of the mode electric field because of the good parallel electron conductivity, it follows from Faraday's law that $K_{\parallel}E_r = \omega B_\theta$, where ω and $K_{\parallel}$ are the mode frequency and parallel component of the wave vector, respectively, E_r is the radial electric field, and B_θ is the poloidal magnetic field. We are thus led naturally to study the stability of high-frequency modes with a finite $K_{\parallel}$, which is our objective in the present work.

II. MODEL AND DISPERSION RELATION

Expecting the high-frequency oscillations to have large phase velocities along the field lines, we assume the background plasma to be cold. The toroidal effects are also ignored, and we are thus left with a bumpy cylinder. By considering only modes with high poloidal mode numbers and mirror ratios that are not too large, the geometrical effects related to the bumpy cylinder may be ignored and a slablike model can be used. We thus employ a cartesian system of coordinates with the unit vectors $\vec{e}_z$ (pointing along the magnetic field lines), $\vec{e}_x$ (in the outward radial direction), and $\vec{e}_y$ ($= \vec{e}_z \times \vec{e}_z$). The effect of the curvature of the field lines is represented by an artificial radial gravitational force acting on the hot electrons with $\vec{g} = v_h^2/R_c\vec{e}_x$, where R_c is the average curvature radius and v_h is the hot electron thermal velocity. To simplify the analysis further, we assume that most of the hot electrons are trapped and that the hot temperature is isotropic.

The perturbation electric and magnetic fields [$\vec{E}(\vec{r})$ and $\vec{B}(\vec{r})$] can be written as $[\vec{E}(x), \vec{B}(x)]\exp[-i(\omega t - ky - k_{\parallel}z)]$, where k is the poloidal component of the wave vector. Denoting the average ring radial location along the minor radius by r_o and the major radius by R_o, it follows that $k = m/r_o$ and $k_{\parallel} = n/R_o$, where m and n are the poloidal and toroidal mode numbers, respectively.

To derive the dispersion relation, we use the quasi-neutrality condition together with the parallel and radial components of Ampere's law. The charge and current densities of the cold background plasma components can be easily evaluated by solving the equations of motion and continuity for each species:

$$-im_j\omega\,\vec{v}_j = e_j(\vec{E} + \vec{v}_j \times \vec{B}_o) \ , \tag{1}$$

$$-i\omega n_j + \vec{\nabla} \cdot (N_j\vec{v}_j) = 0 \ , \tag{2}$$

where m_j is the particle mass, e_j the particle charge, $\vec{v}_j$ the perturbed velocity, n the perturbed density, and N the equilibrium density. To obtain the perturbed charge and current densities of the hot electrons, we have to solve the linearized Vlasov equation for the perturbation in the velocity distribution function. Because of their small number

density and large parallel velocity, we can show that the contribution of the passing hot electrons can be ignored. To obtain the perturbation in the trapped particle distribution function, we assume first that equilibrium distribution of the hot electrons is given by

$$F_h = \frac{N_h}{(2\pi v_h^2)^{3/2}} \exp\left[-(v^2 + 2g_h x)/2v_h^2\right]\left[1 - \left(x - \frac{v_y}{|\Omega_e|}\right)\left(\frac{1}{L_h} + \frac{2}{R_c}\right)\right] , \qquad (3)$$

where L_h is the magnitude of the hot electron density scale length. Using the linearized Vlasov equation, we can then express the perturbation in the trapped electron distribution function in terms of the electric and magnetic perturbations,

$$f_{h,t} = \frac{ieF_h}{k_m v_h^2}\left[E_y + i(\omega - \omega_{*h}) \times \int_{-\infty}^{0} d\tau\, (E_y + v_z' B_x - v_x' B_z)\exp[-i\omega\tau + ik(y' - y) + iK_{\|}(z' - z)]\right] , \qquad (4)$$

where

$$v_x' = v_\perp \sin(\Omega_e \tau + \phi) ,$$

$$v_y' = v_\perp \cos(\Omega_e \tau + \phi) + v_{dh} ,$$

$$v_z^2 = \hat{v}_{\|} \cos(\omega_b \tau + \psi) ,$$

$$y' - y = \frac{v_\perp}{\Omega} \sin(\Omega_e \tau + \phi) - \frac{v_\perp}{\Omega} \sin\phi + v_{dh}\tau ,$$

$$z' - z = \frac{\hat{v}_{\|}}{\omega_b} \sin(\omega_b \tau + \psi) - \frac{\hat{v}_{\|}}{\omega_b} \sin\psi ,$$

where ω_{*h} is the hot electron diamagnetic frequency equal to $kv_h^2\left(1/L_n + 2/R_c\right)/|\Omega_e|$, $\hat{v}_{\|}$ is the magnitude of the parallel velocity at the midplane of the mirror section, ω_b is the parallel bounce frequency, and v_d is the poloidal magnetic drift velocity. Equation (2) may be easily integrated to obtain $f_{h,t}$. The electron gyration and bounce motion will result in two summations over the electron gyro- and bounce frequencies with the proper Bessel function coefficient.[5] Since our analysis is limited to modes whose parallel wave length is much longer than the distance between the throats of a mirror section and since the frequencies considered are much smaller than the electron gyro- and average bounce frequencies, we can write

$$f_h \simeq \frac{ieF_h}{k_m v_h^2}\left[E_y - (\omega - \omega_{*h})\,\frac{\left(E_y - \frac{ikv_\perp^2}{2\Omega_e} B_z\right)\left(1 - \frac{ikv_x}{\Omega_e}\right)}{\omega m \omega_p}\right], \tag{5}$$

where ω_p is the bounce-averaged poloidal magnetic precession frequency. Thus, we note that magnetic bending does not influence the response of the trapped hot electron to lowest order in the long parallel wave length limit. Finite hot electron Larmor radius effects were also ignored in Eq. (5).

We can now evaluate the contribution of the hot electrons to the perturbed charge density and radial and axial components of the current density in terms of the perturbed electric and magnetic fields. Using the quasi-neutrality condition together with Ampere's law, we arrive at the following two coupled, first-order differential equations:

$$AE_x = i\left(C + D\,\frac{d}{dx}\right) E_y\,, \tag{6}$$

$$\left(F + G\,\frac{d}{dx}\right) E_x = i\left(H + I\,\frac{d}{dx}\right) E_y\,, \tag{7}$$

where

$$A = a_1 + \frac{1/\nu}{1 - 1/\nu^2} ,$$

$$C = a_2 \frac{1}{1 - 1/\nu^2} ,$$

$$D = -a_1/r ,$$

$$F = -a_2 + \frac{1 - \delta_i/\nu}{1 - 1/\nu^2} ,$$

$$G = \left[\frac{1/\nu}{1 - 1/\nu^2} + K_{\|}^2 v_A^2/(\Omega_i^2 \nu)\right] R ,$$

$$H = -a_3 + \frac{\delta_i}{1 - 1/\nu^2} - kG ,$$

$$I = \left[a_2 - 1/(1 - 1/\nu^2)\right]/k ,$$

$$a_1 = \frac{k^2 v_A^2}{\nu \Omega_i'} \left[1 + \frac{K_{\|}^2}{k^2} + \frac{\beta_h}{2} \left(\frac{\nu}{q} - \frac{1}{2\varepsilon_h}\right)\right] ,$$

$$a_2 = \alpha - \alpha \left(\frac{\nu}{q} - \frac{1}{2\varepsilon_h}\right) U_2 ,$$

$$a_3 = 2\alpha\delta_h\varepsilon_h \left(\frac{\nu}{q} - \frac{1}{2\varepsilon_h}\right)\left(bU_2 - \frac{U_1}{2}\right) .$$

The indices i, e, and h denote the ions, electrons, and hot electrons, respectively; $\alpha = N_h(x)/N_i(x)$; $\nu = \omega/\Omega_i$; v_A is the Alfvèn speed equal to $\left[B^2/(\mu_o N m_i)\right]^{1/2}$; $\beta_h = 2\mu_o N_h T_h/B_o^2$; $\delta_j = 1/kL_{n,j}$; and $\varepsilon_j = L_{n,j}/R_c$. We also note that

$$U_s = \int_0^\infty dx \frac{e^{-\chi} x^{s-1}}{\nu/q - \frac{1}{2} - \left(b - \frac{1}{2}\right)x} ,$$

where $q = 2km_e v_h^2/(eB_o R_c \Omega_i)$ is the ratio of the average hot electron magnetic drift frequency in the vacuum magnetic field to the ion cyclotron frequency and $b = 1 - \beta_h/4\epsilon$ is the ratio of the average hot electron magnetic drift frequency to its value in the vacuum field.

III. ANALYSIS

Equations (6) and (7) can be solved numerically for any general density distribution. Our main interest in the present work is to describe the new features introduced by magnetic field line bending. We thus make the approximation $U_s \simeq 1/(\nu/q - b)$, which allows us to proceed analytically and which was justified by comparing the analytical results with the numerical computations.

It is also not difficult to see that Eqs. (6) and (7) can be easily reduced to a single second-order differential equation for E_y. The coefficient of the second derivative vanishes when either G or D is equal to zero. This situation gives rise to branch points that are related to the presence of a shear Alfvèn resonance ($G = 0$) and a precession-wave resonance ($\nu/q = 1$ when $D = 0$ and $K_\parallel k \ll 1$).

An incident wave satisfying the resonance condition can undergo a strong damping at the resonance layer as has already been shown in studies related to shear Alfvèn heating.[6] The precession-wave resonance thus represents the possibility of ring heating by an external rf source. Using a cylindrical version of Eqs. (6) and (7) and taking into account the presence of a driving antenna, we have confirmed this possibility.[7]

Discrete radially localized shear Alfvèn waves can be extracted from Eqs. (6) and (7) for a "ringless" plasma.[8,9] For such modes, $\omega - K_\parallel v_A$ is finite across the whole profile, resulting in globally extended modes. Such modes can interact with the electron ring, and recent studies have shown that an instability can develop when $m\omega_p \simeq K_\parallel v_A$.[2] Our main interest, here, is to study modes whose frequency exceeds the ion cyclotron frequency. If such modes are

strongly localized radially within the outer part of the ring, we can then combine Eqs. (6) and (7) in the following simple form:

$$\left(1 + \frac{K_{\|}^2 v_A^2}{\Omega_i^2}\right)\left(\frac{-E_y''}{k^2} + E_y\right) = \left(\frac{\alpha\delta\nu}{\frac{\nu}{q} - 1} + \delta\nu\right) E_y \ . \tag{8}$$

In deriving Eq. (8), we have kept only the dominant terms and have assumed that $\nu >> 1$ and that all plasma components have the same scale length in the outer part of the ring.

Equation (8) is identical to Eq. (6) of Ref. 3 except for the appearance of the factor $\left(1 + K_{\|}^2 v_A^2/\Omega_i^2\right)$, caused by magnetic bending. That localized modes exist can be seen by allowing for the presence of an inflection point in the density profile. In the limit $kL_n > 1$, the solution to Eq. (8) can be written as

$$(\nu - q)\left[\nu - \frac{k_{\perp}^2}{k^2\delta}\left(1 + \frac{K_{\|}^2 v_A^2}{\Omega_i^2}\right)\right] = -\alpha\nu q \ , \tag{9}$$

where $k_{\perp}^2 = k^2 + \frac{(2n + 1)k}{L_n}$, $n = 0, 1, \ldots$. When $K_{\|} = 0, \alpha$, the ratio of the hot electron to the ion densities has to exceed a certain threshold for the hot interchange instability to be triggered. This action is caused by the weak coupling between the precessional wave and the high-frequency drift branch, due to the significant frequency separation. Allowing for the magnetic bending increases the coupling between the two modes because of the introduced $K_{\|}$ dispersion. The condition for the instability becomes

$$\alpha > \left[1 - \frac{k_{\perp}}{k}\left(\frac{1 + K_{\|}^2 v_A^2/\Omega_i^2}{\delta q}\right)^{1/2}\right]^2 \ . \tag{10}$$

If $K_{\|}$ is set equal to zero, we then recover the instability condition for the hot electron interchange mode. When $K_{\|}$ is finite, an instability is possible for any finite α. If we let $\delta q = 5$, the ion

density at the ring location equal 5×10^{11} cm^{-3}, $R_c = 1.5$ m, and $k_\perp^2 \simeq 2k^2$, we find that there is an unstable window in the $K_\parallel$-spectrum centered around $n \simeq 7$. The number of unstable modes increases with $\propto$ according to Eq. (10). The real frequency of the unstable mode is only weakly dependent on $K_\parallel$ and is approximately given by $\omega_r = 2mv_h^2/(R_c|\Omega_e|)$. The maximum growth rate follows from Eq. (8) and is given approximately by $\sqrt{\alpha}\omega_r$. We may also note the weak dependence of the instability threshold on the poloidal mode number. A stronger dependence is expected when one allows for the hot electron finite Larmor radius effects and the cylindrical effects on modes with low poloidal mode numbers. In Fig. 1 we show the typical $\omega - K_\parallel$ dispersion

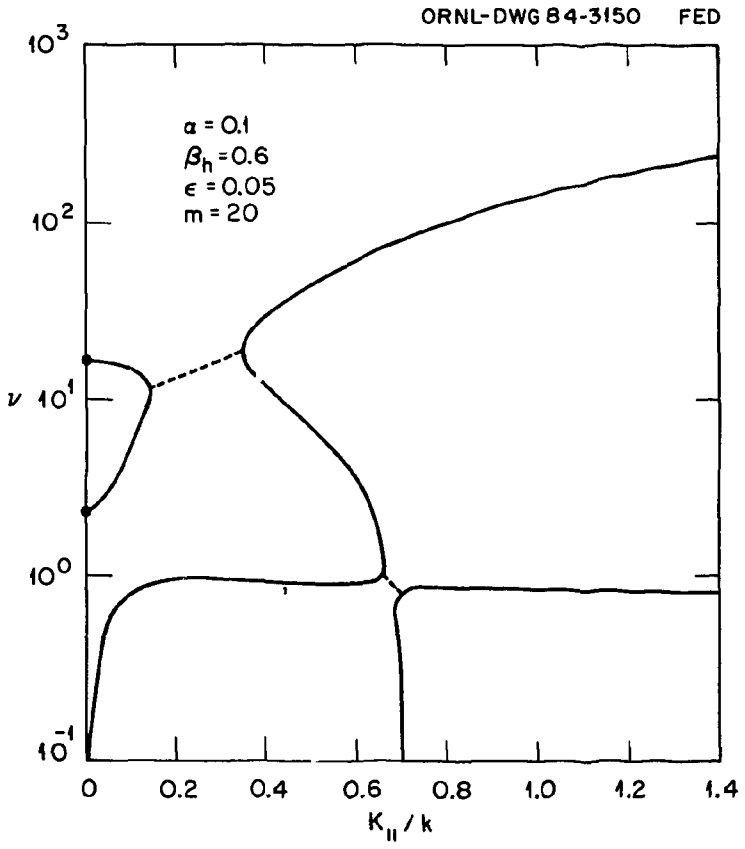

Fig. 1. The local $\omega - K_\parallel$ dispersion based on Eqs. (6) and (7) for $\alpha = 0.1$, $\beta_h = 0.6$, $\varepsilon = 0.05$, $m = 20$, $R_o = 1.5$ m, and $r_o = 0.1$ m.

based on the local limit of Eqs. (6) and (7). The dashed portions represent instabilities, with the higher frequency being the one discussed previously and the lower one being the shear Alfvèn instability, which is related to the precessional modes studied recently in the eikonal limit.[2]

IV. DISCUSSION AND CONCLUSIONS

As mentioned before, high-frequency fluctuations were observed experimentally in the EBT before the hot electron density was high enough to trigger the hot interchange mode. Magnetic probes located near the vacuum wall detected both poloidal and axial high-frequency fluctuations in the range 40 to 75 megacycles/s. Since the component of the magnetic perturbation normal to the vacuum wall ($B_{r,w}$) must vanish, it follows from $\vec{\nabla} \cdot \vec{B} = 0$ that $B_{z,w}/B_{\theta,w} = k/K_{\|}$, where $B_{z,w}$ and $B_{\theta;w}$ denote the axial and poloidal components, respectively, of the magnetic perturbation at the wall. The sensitivity of the ratio of B_z to B_θ to the radial location demands an accurate numerical computation of the radial profile of the perturbations. Assuming a poloidal magnetic precession frequency of 6 megacycles/s and identifying the observed fluctuations with the modes discussed above, it follows that $6 < m < 13$. A more positive identification would require an experimental determination of the parallel and poloidal mode numbers related to the fluctuations.

In conclusion, we have shown that the coupling between the hot electron precessional wave and the finite $K_{\|}$ high-frequency surface wave can lead to instabilities at any finite hot electron density. This discovery may explain some of the high-frequency fluctuations observed during the experimental period.

REFERENCES

[1] D. L. Hillis, G. R. Haste, and L. A. Berry, Phys. Fluids 26, 820 (1983).

[2] D. E. Baldwin and H. L. Berk, Phys. Fluids 26, 3595 (1983).

[3] A. M. El-Nadi, Phys. Fluids 25, 2019 (1982).

[4] H. L. Berk, J. W. Van Dam, M. N. Rosenbluth, and D. A. Spong, Phys. Fluids 26, 201 (1983).

[5] A. M. El-Nadi, in Modern Plasma Physics (International Atomic Energy Agency, Vienna, 1981).

[6] W. Grossmann and J. Tataronis, Z. Phys. 61, 217 (1973).

[7] A. M. El-Nadi, K. Appert, and J. C. Whitson (personal communication).

[8] K. Appert, R. Gruber, F. Troyon, and J. Vaclavik, Plasma Phys. 24, 1147 (1982).

[9] S. M. Mahajan, D. W. Ross, and G. L. Chen, Phys. Fluids 26, 2195 (1983).

ORNL/TM-9369
Dist. Category UC-20

INTERNAL DISTRIBUTION

1. D. L. Akers
2. L. A. Berry
3. B. A. Carreras
4. R. A. Dory
5–9. A. M. El-Nadi
10. C. L. Hedrick
11–12. S. Hiroe
13. S. P. Hirshman
14. E. F. Jaeger
15. L. W. Owens
16. J. Sheffield
17. D. A. Spong
18. J. S. Tolliver
19–20. J. C. Whitson
21–22. Laboratory Records Department
23. Laboratory Records ORNL-RC
24. Document Reference Section
25. Central Research Library
26. Fusion Energy Division Library
27–28. Fusion Energy Division Publications Office
29. ORNL Patent Office

EXTERNAL DISTRIBUTION

31–32. H. F. Hassan, Cairo University, Giza, Egypt
33–34. H. A. Kirolous, Cairo University, Giza, Egypt
35. Office of the Assistant Manager for Energy Research and Development, U.S. Department of Energy, Oak Ridge Operations, Box E, Oak Ridge, TN 37831
36. J. D. Callen, Department of Nuclear Engineering, University of Wisconsin, Madison, WI 53706
37. R. W. Conn, Department of Chemical, Nuclear, and Thermal Engineering, University of California, Los Angeles, CA 90024
38. S. O. Dean, Director, Fusion Energy Development, Science Applications International Corporation, 2 Professional Drive, Gaithersburg, MD 20879
39. H. K. Forsen, Bechtel Group, Inc., Research Engineering, P.O. Box 3965, San Francisco, CA 94105
40. J. R. Gilleland, GA Technologies, Inc., Fusion and Advanced Technology, P.O. Box 81608, San Diego, CA 92138
41. R. W. Gould, Department of Applied Physics, California Institute of Technology, Pasadena, CA 91125
42. R. A. Gross, Plasma Research Laboratory, Columbia University, New York, NY 10027
43. D. M. Meade, Plasma Physics Laboratory, Princeton University, P.O. Box 451, Princeton, NJ 08544
44. W. M. Stacey, Jr., School of Nuclear Engineering, Georgia Institute of Technology, Atlanta, GA 30332
45. D. Steiner, Rensselaer Polytechnic Institute, Nuclear Engineering Department, NES Building, Tibbets Avenue, Troy, NY 12181

46. R. Varma, Physical Research Laboratory, Navrangpura, Ahmedabad 380009, India
47. Bibliothek, Max-Planck Institut für Plasmaphysik, D-8046 Garching, Federal Republic of Germany
48. Bibliothek, Institut für Plasmaphysik, KFA, Postfach 1913, D-5170 Jülich, Federal Republic of Germany
49. Bibliotheque, Centre de Recherches en Physique des Plasmas, 21 Avenue des Bains, 1007 Lausanne, Switzerland
50. Bibliotheque, Service du Confinement des Plasmas, CEA, B.P. 6, 92 Fontenay-aux-Roses (Seine), France
51. Documentation S.I.G.N., Departement de la Physique du Plasma et de la Fusion Controlee, Centre d'Etudes Nucleaires, B.P. No. 85, Centre du Tri, 38041 Cedex, Grenoble, France
52. Library, Culham Laboratory, UKAEA, Abingdon, Oxfordshire, OX14 3DB, England
53. Library, FOM Instituut voor Plasma-Fysica, Rijnhuizen, Jutphaas, The Netherlands
54. Library, Institute of Plasma Physics, Nagoya University, Nagoya 64, Japan
55. Library, International Centre for Theoretical Physics, Trieste, Italy
56. Library, Laboratorio Gas Ionizzati, Frascati, Italy
57. Library, Plasma Physics Laboratory, Kyoto University, Gokasho, Uji, Kyoto, Japan
58. Plasma Research Laboratory, Australian National University, P.O. Box 4, Canberra, A.C.T. 2000, Australia
59. Thermonuclear Library, Japan Atomic Energy Research Institute, Tokai, Naka, Ibaraki, Japan

60–167. Given distribution as shown in TIC-4500, Magnetic Fusion Energy (category UC-20)